Polar warming in the Mars thermosphere: Seasonal variations owing to changing insolation and dust distributions

S. W. Bougher,[1] J. M. Bell,[1] J. R. Murphy,[2] M. A. Lopez-Valverde,[3] and P. G. Withers[4]

Received 13 July 2005; revised 16 December 2005; accepted 27 December 2005; published 27 January 2006.

[1] Warming of the martian lower thermosphere (100–130 km) at north polar latitudes near the perihelion/winter solstice (Ls = 270) was recently observed. No analogous warming has been observed within the south polar thermosphere during its aphelion/winter season (Ls ~ 90). Detailed global model simulations are required to investigate the physical processes driving these seasonal variations. New simulations are conducted for conditions approximating the atmosphere during these Mars Global Surveyor (MGS) and Odyssey (ODY) aerobraking periods. Strong northern winter polar warming features are calculated near 120 km, yielding nightside mean temperatures 10–15 K warmer than observed ODY values. No southern winter polar warming trend is simulated; however, nightside mean temperatures are 20–30 K warmer than observed by MGS. The stronger interhemispheric circulation during northern winter is clearly driven by stronger insolation and dust heating near perihelion, resulting in subsidence and warmer temperatures in the northern polar night. **Citation:** Bougher, S. W., J. M. Bell, J. R. Murphy, M. A. Lopez-Valverde, and P. G. Withers (2006), Polar warming in the Mars thermosphere: Seasonal variations owing to changing insolation and dust distributions, *Geophys. Res. Lett.*, *33*, L02203, doi:10.1029/2005GL024059.

1. Background and Motivation

[2] Recent Mars Global Surveyor (MGS) and Mars 2001 Odyssey (ODY) Accelerometer measurements have provided a significant increase in the thermospheric databases available to characterize the Mars upper atmospheric structure and dynamics [e.g., *Keating et al.*, 1998, 2003; *Withers et al.*, 2003]. Initial analysis of these aerobraking data sets confirms a strong coupling of the Mars lower and upper atmospheres that is composed of: (1) seasonal and dust-driven inflation/contraction of the entire atmosphere, (2) dynamical forcing from migrating and non-migrating tides propagating upward from the Mars lower atmosphere [e.g., *Forbes et al.*, 2002; *Wilson*, 2002; *Withers et al.*, 2003; *Bougher et al.*, 2004; *Angelats i Coll et al.*, 2004, 2005], and (3) strong interhemispheric circulation during solstice conditions [e.g., *Keating et al.*, 2003]. Nevertheless, the temporal and spatial coverage afforded by these aerobraking measurements is quite limited [e.g., *Withers et al.*, 2003]. At the present time, coordinated use of three-dimensional (3-D) lower to upper atmosphere Mars models is vital to the global characterization and diagnostic understanding of the Martian thermospheric structure and dynamics.

[3] Near the end of MGS Phase 2 aerobraking (January to February 1999), sampling by the Accelerometer occurred during southern winter solstice, aphelion conditions (Ls = 70–90). MGS periapsis rapidly shifted from ~1500 hours (dayside) to 0200 hours (nightside) as the spacecraft passed over the southern pole. Figure 1 illustrates the Accelerometer derived temperatures that were obtained near 120 km during this day-to-night transition. Polar warming features do not exist; temperatures near 120 km increase slightly from the equator (130–140 K) toward mid-latitudes (up to 160 K), while dropping to 100 K near the South pole.

[4] From October 2001 to January 2002, the Mars ODY Accelerometer sampled high northern latitudes during aerobraking (Ls = 265–310) [*Keating et al.*, 2003; *Tolson et al.*, 2005]. Now with the passage of periapsis over the northern winter pole, the spacecraft position rapidly shifted from ~1700 hours (dayside) to 0200–0300 hours (nightside). No global or regional dust storms erupted during this northern winter period. However, as a result of the final waning stage of the 2001 global dust storm [e.g., *Liu et al.*, 2003], the ~25 km altitude atmospheric temperature during ODY aerobraking was still 3–5 K warmer than it had been the preceding Martian year [*Smith*, 2004].

[5] The most surprising feature observed in ODY aerobraking data in the northern winter night was a strong polar warming over 100–130 km [e.g., *Keating et al.*, 2003]. Temperatures near periapsis (100–110 km) were discovered to increase with latitude (60–90N) from about 100 to 170–200 K, maximizing near the North pole on the nightside. Corresponding temperatures near 120 km were observed to increase from 110 K to 160–170 K as the North pole was approached. These ODY Accelerometer observations provide the first clear evidence of strong winter polar warming at Mars thermospheric heights [*Keating et al.*, 2003]. However, there was no concurrent lower atmosphere polar warming observed during this ODY aerobraking period [e.g., *Smith*, 2004].

[6] Lower atmosphere (25–80 km) north polar winter warming has previously been observed during several events [e.g., *Deming et al.*, 1986; *Jakosky and Martin*, 1987; *Theodore et al.*, 1993]. Recently, *Smith et al.* [2001] also indicated enhanced north winter polar temperatures above 50 km in the MGS Thermal Emission Spectrometer (TES) limb data. Winter polar warming in the lower atmosphere for specific events was realistically simulated using revised Mars lower atmosphere models that were extended to ~90 km or more [cf. *Wilson*, 1997; *Forget*

[1]Department of Atmospheric, Oceanic, and Space Sciences, University of Michigan, Ann Arbor, Michigan, USA.
[2]Department of Astronomy, New Mexico State University, Las Cruces, New Mexico, USA.
[3]Instituto de Astrofisica de Andalucia, Consejo Superior de Investigaciones Científicas, Granada, Spain.
[4]Center for Space Physics, Boston University, Boston, Massachusetts, USA.

0094-8276/06/2005GL024059$05.00

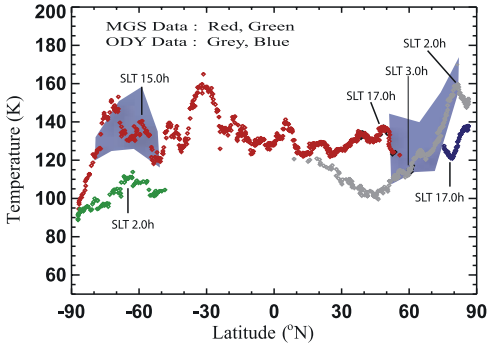

Figure 1. Latitudinal, seasonal and diurnal temperature (K) variations at 120 km, derived from Accelerometer data sets. Winter polar warming features are contrasted for the two observing seasons near aphelion (Ls = 90) and perihelion (Ls = 270). Blue shaded regions correspond to MGCM-MTGCM simulated nightside (0200–0300 hour) temperatures and their variations over longitude.

et al., 1999]. Such an extension enabled these models to capture the diabatically driven interhemispheric (Hadley) circulation that is strong and deep on Mars, spanning the region from the ground to nearly 100 km. Strong meridional winds above 50 km lead to a horizontal convergence of mass and downward motion above the polar region, resulting in adiabatic warming down to ~25 km. This warming is shown to be most pronounced during perihelion conditions (Ls = 270), when maximum solar insolation and strong dust heating prevail. Gravity wave momentum forcing is not required to simulate this polar warming of the Mars lower atmosphere. This is a departure from the situation in the Earth's middle atmosphere where winter polar warming requires gravity wave momentum forcing to slow zonal winds and accelerate meridional winds [e.g., *Holton*, 1982].

[7] The winter polar warming in the Mars thermosphere may similarly occur as a result of adiabatic heating from the subsiding branch of a strong interhemispheric circulation cell during the solstices. This circulation pattern should be enhanced during the perihelion season by the remote effects of significant (and highly variable) aerosol heating in the lower atmosphere [*Keating et al.*, 2003].

[8] Detailed global model simulations are needed to capture the energetics and dynamics of the combined lower and upper atmospheres in order to address this issue of Mars thermospheric winter polar warming and its hemispheric variations. Coupled yet separate General Circulation Models (GCMs) of the lower and upper atmospheres of Mars are now used to address these features and the underlying dynamical processes linking these Mars atmospheric regions.

2. MTGCM-MGCM Coupled Models

[9] The Mars Thermospheric General Circulation Model (MTGCM) itself is a finite difference primitive equation model that self-consistently solves for time-dependent neutral temperatures, neutral-ion densities, and three component neutral winds over the globe [see *Bougher et al.*, 1999, 2004]. MTGCM prognostic and diagnostic thermospheric fields are simulated on 33-pressure levels (at altitudes above 1.32 μbar corresponding to ~70–300 km), with a 5 × 5° latitude and longitude resolution. Recently, a fast non-Local Thermodynamic Equilibrium (NLTE) 15-micron cooling scheme was implemented in the MTGCM, along with corresponding near-IR heating rates. These improvements are based upon recent detailed one dimensional (1-D) NLTE model calculations for the Mars upper atmosphere from M. A. Lopez-Valverde (private communication, 2005).

[10] The MTGCM is currently driven from below by the NASA Ames Mars General Circulation Model (MGCM) code [e.g., *Haberle et al.*, 1999] at the 1.32 μbar level (near 60–80 km), permitting a detailed coupling across this boundary. This coupling scheme captures both migrating and non-migrating upward propagating tides plus the thermal expansion and contraction of the Mars lower atmosphere with the passage of the seasons and dust storm events [see *Bougher et al.*, 2004]. Key prognostic (temperatures, zonal and meridional winds) and diagnostic (geopotential height) fields are passed upward from the MGCM to the MTGCM at the 1.32-μbar pressure surface at every MTGCM grid point on 2-minute time step intervals. No downward coupling from the MTGCM to the MGCM is presently activated. However, simulated lower atmosphere warming is still achievable [e.g., *Forget et al.*, 1999; *Wilson*, 1997] with a deep enough model domain (which is included within the Ames MGCM) and the appropriate thermodynamic forcing. The inclusion of the Ames MGCM in providing a realistic lower atmosphere is critical for achieving an improved simulation of the Mars upper atmosphere within the MTGCM domain.

[11] Specific MGCM-MTGCM model inputs are prescribed for two cases corresponding to MGS (aphelion) and ODY (perihelion) sampling periods during which opposite polar night regions were traversed. For the former, Ls = 90 (season), F10.7-cm = 100 (solar flux index), and $\tau \sim 0.3$ (average vertically integrated visible dust opacity) parameters are specified. A globally uniform horizontal dust distribution is assumed for the aphelion case. For perihelion, the detailed horizontal dust opacity distribution is obtained from the MGS TES observations for TES Year 3 (as defined by *Liu et al.* [2003]). A factor of 2 is used to scale IR to visible integrated dust opacity values. For perihelion, Ls = 270 and F10.7-cm = 175 (solar maximum) parameters are specified; visible opacity values achieve a global average of ~1.0.

[12] The vertical dust distributions for the two simulations are prescribed making use of the Conrath parameter (CR) [*Conrath*, 1975], which defines a pressure to which dust is essentially well mixed, with a decreasing mixing ratio above this level. For the aphelion dust distribution employed in our simulations (CR = 0.3), dust is well mixed in the bottom atmospheric scale height ("shallow" mixing up to ~10 km). Above this level, the dust mixing ratio declines to 50% of the surface value at 2 scale heights. However, for perihelion, the depth of vertical mixing is permitted to vary locally with the TES horizontal dust distribution, so that the deepest mixing regions (up to ~50 km) correspond to the largest integrated dust opacities ($\tau = 1.3$). This latter dust distribution is key to providing an improved MGCM-MTGCM simulation of the perihelion season winter polar warming

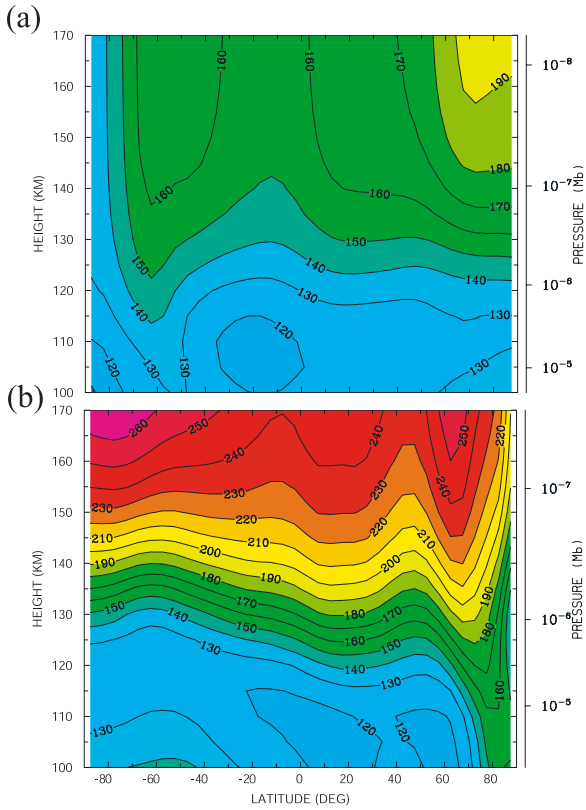

Figure 2. MGCM-MTGCM zonal averaged temperature slices as a function of height and latitude: (a) Ls = 90 and (b) Ls = 270. Contour intervals are 10 K. Color shading is coordinated between these plots.

over previous simulations using the MTGCM alone [see *Keating et al.*, 2003].

3. Model Results and Data Comparisons

[13] Figure 2 represents coupled MGCM-MTGCM model results corresponding to the seasonal conditions appropriate for MGS and ODY aerobraking. Zonal averaged temperature slices are presented in order to capture the mean structure of the polar warming features above 100 km. A reference altitude of 120 km is chosen for discussion, since this level is close to most spacecraft periapsis altitudes where scale heights and temperatures can be easily derived.

[14] Figure 2a shows southern hemisphere polar temperatures that decrease overall from 60–90S, ranging from 145 to 128 K near the pole. No thermospheric polar warming is simulated, in accord with MGS aerobraking data. However, these simulated mean temperatures are up to 20–25 K warmer than day-night averages of MGS temperatures shown in Figure 1. Lower atmosphere (~25 km) temperatures are calculated to be ~140 K in this polar region, similar to MGS TES data. Thermospheric densities at 120 km (not shown) are calculated to drop by a factor of three from the equator to the South pole.

[15] Conversely, Figure 2b shows zonal averaged perihelion temperature variations. Notice that a strong warming (ΔT = +30–40 K) is present in the northern polar region (60–90N), with near polar temperatures approaching 170 K. This simulated mean temperature is ~30 K warmer than the day-night average of ODY temperatures shown in Figure 1. Lower atmosphere temperatures show little polar warming. The corresponding thermospheric polar densities (not shown) vary little from the equator to the North polar region, consistent with this temperature structure.

[16] Alternatively, simulated nightside temperatures are illustrated in Figure 1. Calculated longitude variations at 0200–0300 hours are presented for both cases using shaded blue regions. Note that northern winter polar temperatures span available observations, with nightside mean temperatures only ~10–15 K warmer than observed ODY values. Conversely, even though no southern winter polar warming trend is simulated, nightside mean temperatures are 20–30 K warmer than observed by MGS. Tidally produced diurnal temperature amplitudes are calculated to be as large as ±17–22 K for both cases.

[17] What dynamical processes drive this polar warming and the seasonal differences presented above? Figure 3 illustrates zonally averaged slices of dynamical heating terms for the same MGS and ODY cases. Superimposed stream function curves trace the corresponding mean flow patterns. Maximum zonal averaged meridional winds (not shown) are −105 m/sec for aphelion and +165 m/sec for perihelion conditions; that is, the summer-to-winter interhemispheric circulation during perihelion is much stronger.

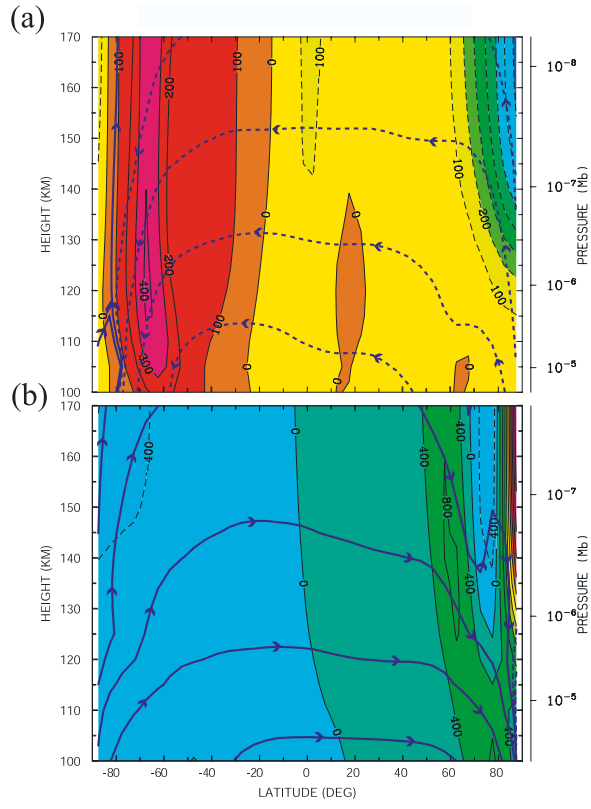

Figure 3. MGCM-MTGCM zonal averaged adiabatic heating (K/day) slices as a function of height and latitude: (a) Ls = 90 and (b) Ls = 270. Maximum heating is indicated by the red color: 400 K/day (Figure 3a) and ~3000K K/day (Figure 3b). Stream function (dark blue) lines are superimposed to indicate the direction of the interhemispheric flow patterns, i.e., southward (dashed, Figure 3a) and northward (solid, Figure 3b).

Adiabatic heating resulting from subsiding flow dominates in both polar night regions (±60–90 latitude). At 120 km and above, this heating reaches ~300–400 K/day during aphelion (Figure 3a) versus ~400–1000 K/day during perihelion (Figure 3b) polar night conditions. Furthermore, strong adiabatic heating is also concentrated for perihelion conditions closest to the northern pole (800–3000 K/day). The basic features of the martian winter polar warming are thus controlled by seasonal changes in the strength of the Hadley circulation.

4. Conclusions and Implications

[18] In-situ Martian thermospheric observations obtained by aerobraking spacecraft indicate that thermospheric polar warming is much stronger during perihelion than aphelion conditions. The details of this warming are important for controlling polar densities at aerobraking altitudes. The stronger interhemispheric (Hadley) circulation during northern winter is clearly driven by the stronger insolation and dust heating near perihelion. Current simulations demonstrate that the basic features of the martian thermospheric winter polar warming are controlled by these seasonal changes in the solar plus tidal forcing, the corresponding variations in the strength of the Hadley circulation, and the resulting changes in the magnitude of the adiabatic heating near the winter poles. Calculations of polar warming show that perihelion adiabatic heating can be more than twice as strong as that for aphelion. However, simulated polar night temperatures are somewhat warmer than observed, indicating that the corresponding meridional flow is too strong. These simulations presently neglect any parameterized small scale (orographic) gravity wave effects [see *Angelats i Coll et al.*, 2005]. Their incorporation may ultimately slow these meridional winds and reduce the magnitude of the winter polar warming. Further studies are needed. Finally, interannual variations in dust distributions near perihelion are expected to contribute to significant year-to-year variations in northern polar warming and resulting temperatures and densities.

[19] **Acknowledgments.** We are grateful to the National Center for Atmospheric Research (NCAR) for the use of the IBM/SP supercomputer resources. Special thanks also go to Ben Foster of NCAR for his help developing the MGCM-MTGCM coupler code.

References

Angelats i Coll, M., F. Forget, M. A. López-Valverde, P. L. Read, and S. R. Lewis (2004), Upper atmosphere of Mars up to 120 km: Mars Global Surveyor accelerometer data analysis with the LMD general circulation model, *J. Geophys. Res.*, *109*, E01011, doi:10.1029/2003JE002163.

Angelats i Coll, M., F. Forget, M. A. López-Valverde, and F. Gonzalez-Galindo (2005), The first Mars thermospheric general circulation model: The Martian atmosphere from the ground to 240 km, *Geophys. Res. Lett.*, *32*, L04201, doi:10.1029/2004GL021368.

Bougher, S. W., S. Engel, R. G. Roble, and B. Foster (1999), Comparative terrestrial planet thermospheres: 2. Solar cycle variation of global structure and winds at equinox, *J. Geophys. Res.*, *104*, 16,591–16,611.

Bougher, S. W., S. Engel, D. P. Hinson, and J. R. Murphy (2004), MGS Radio Science electron density profiles: Interannual variability and implications for the neutral atmosphere, *J. Geophys. Res.*, *109*, E03010, doi:10.1029/2003JE002154.

Conrath, B. J. (1975), Thermal structure of the Martian atmosphere during the dissipation of the dust storms of 1971, *Icarus*, *24*, 36–46.

Deming, D., et al. (1986), Polar warming in the middle atmosphere of Mars, *Icarus*, *66*, 366–379.

Forbes, J. M., A. F. C. Bridger, S. W. Bougher, M. E. Hagan, J. L. Hollingsworth, G. M. Keating, and J. Murphy (2002), Nonmigrating tides in the thermosphere of Mars, *J. Geophys. Res.*, *107*(E11), 5113, doi:10.1029/2001JE001582.

Forget, F., F. Hourdin, R. Fournier, C. Hourdin, O. Talagrand, M. Collins, S. R. Lewis, P. L. Read, and J.-P. Huot (1999), Improved general circulation models of the Martian atmosphere from the surface to above 80 km, *J. Geophys. Res.*, *104*, 24,155–24,175.

Haberle, R. M., M. M. Joshi, J. R. Murphy, J. R. Barnes, J. T. Schofield, G. Wilson, M. Lopez-Valverde, J. L. Hollingsworth, A. F. C. Bridger, and J. Schaeffer (1999), General circulation model simulations of the Mars Pathfinder atmospheric structure investigation/meteorology data, *J. Geophys. Res.*, *104*, 8957–8974.

Holton, J. R. (1982), The role of gravity wave induced drag and diffusion in the momentum budget of the mesosphere, *J. Atmos. Sci.*, *39*, 791–799.

Jakosky, B. M., and T. Z. Martin (1987), Mars: North polar atmospheric warming during dust storms, *Icarus*, *72*, 528–534.

Keating, G. M., et al. (1998), The structure of the upper atmosphere of Mars: In-situ accelerometer measurements from Mars Global Surveyor, *Science*, *279*, 1672–1676.

Keating, G. M., et al. (2003), Brief review on the results obtained with the MGS and Mars Odyssey 2001 Accelerometer Experiments, paper presented at International Workshop: Mars Atmosphere Modeling and Observations, Inst. de Astrofis. de Andalucia, Granada, Spain, 13–15 Jan.

Liu, J., M. I. Richardson, and R. J. Wilson (2003), An assessment of the global, seasonal, and interannual spacecraft record of Martian climate in the thermal infrared, *J. Geophys. Res.*, *108*(E8), 5089, doi:10.1029/2002JE001921.

Smith, M. D. (2004), Interannual variability in TES atmospheric observations of Mars during 1999–2003, *Icarus*, *167*, 148–165.

Smith, M. D., J. C. Pearl, B. J. Conrath, and P. R. Christensen (2001), Thermal Emission Spectrometer results: Atmospheric thermal structure and aerosol distribution, *J. Geophys. Res.*, *106*, 23,929–23,945.

Theodore, B., et al. (1993), Solstial temperature inversions in the Martian middle atmosphere: Observational clues and 2-D modeling, *Icarus*, *105*, 512–528.

Tolson, R. H., et al. (2005), Application of accelerometer data to Mars Odyssey aerobraking and atmospheric modeling, *J. Spacecraft Rockets*, *42*, 435–443.

Wilson, R. J. (1997), A general circulation model of the Martian polar warming, *Geophys. Res. Lett.*, *24*, 123–126.

Wilson, R. J. (2002), Evidence for nonmigrating thermal tides in the Mars upper atmosphere from the Mars Global Surveyor Accelerometer Experiment, *Geophys. Res. Lett.*, *29*(7), 1120, doi:10.1029/2001GL013975.

Withers, P. G., S. W. Bougher, and G. M. Keating (2003), The effects of topographically-controlled thermal tides in the Martian upper atmosphere as seen by the MGS accelerometer, *Icarus*, *164*, 14–32.

J. M. Bell and S. W. Bougher, Department of Atmospheric, Oceanic, and Space Sciences, University of Michigan, Ann Arbor, MI 48109-2143, USA. (bougher@umich.edu)

M. A. Lopez-Valverde, Instituto de Astrofisica de Andalucia, CSIC, P.O. Box 3004, E-18080 Granada, Spain.

J. R. Murphy, Department of Astronomy, New Mexico State University, Las Cruces, NM 88003, USA.

P. G. Withers, Center for Space Physics, Boston University, Boston, MA 02215, USA.